Liquid distribution and cohesion in wet granular assemblies beyond the capillary bridge regime

2008 J. Phys.: Condens. Matter 20 494236

(http://iopscience.iop.org/0953-8984/20/49/494236)

J. Phys.: Condens. Matter **20** (2008) 494236 (7pp) doi:10.1088/0953-8984/20/49/494236

Liquid distribution and cohesion in wet granular assemblies beyond the capillary bridge regime

M Scheel[1], R Seemann[1,2], M Brinkmann[1], M Di Michiel[3], A Sheppard[4] and S Herminghaus[1]

[1] MPI for Dynamics and Self-Organization, Bunsenstraße 10, D-37073 Göttingen, Germany
[2] Saarland University, Experimental Physics, D-66041 Saarbrücken, Germany
[3] European Synchrotron Radiation Facility, BP 200, F-38043 Grenoble, France
[4] Department of Applied Mathematics, Australian National University, Canberra ACT 0200, Australia

E-mail: stephan.herminghaus@ds.mpg.de

Received 8 September 2008
Published 12 November 2008
Online at stacks.iop.org/JPhysCM/20/494236

Abstract

Dry sand turns into a stiff and moldable material as soon as it is mixed with some liquid. This is a direct consequence of the internal liquid–air interfaces spanning between the grains which causes capillary cohesion by virtue of the surface tension of the liquid. As a model for wet granulates we investigated random packings of submillimeter spherical beads mixed with water. Measurements of the tensile strength and the fluidization threshold demonstrate that the mechanical stiffness is rather insensitive to the liquid content over a wide range. Only for a high liquid content, when more than half of the available pore space is filled with liquid, does the capillary cohesion weaken. In order to understand the interplay between the mechanical properties and the liquid content, we investigated the liquid distribution in random packings of glass spheres by means of x-ray microtomography. The three-dimensional images reveal that the liquid forms a network of capillary bridges fused at local triangular bead configurations. The spontaneous organization of the liquid into these ramified structures, which exhibit a large liquid–air interface, is responsible for the constancy of the cohesive forces in a wide range of liquid contents beyond the onset of capillary bridge coalescence.

(Some figures in this article are in colour only in the electronic version)

1. Introduction

It is a common experience that a mixture of sand (which in most cases consists of quartz grains) and water makes a moldable material, with sufficient stiffness to build, e.g., sand-castles. At small liquid content, this mechanical stability can be explained by the presence of numerous small water necks (bridges) which form at the contacts between adjacent grains [1–5]. Assuming grains with a rounded shape, one can show by simple geometric arguments that the force induced by such capillary bridges is almost volume independent [6–8]. This conforms to the observation that the cohesive stress depends weakly on the liquid content at small liquid saturations [9–14].

Quite surprisingly the plateau of mechanical stability extends by far the range of liquid contents where the liquid is solely present as individual capillary bridges [15–17]. Above a certain liquid content, the local packing geometry of the grains does not permit the formation of isolated bridges. In this range of liquid content, large changes in the liquid morphology must take place in the granular assembly as more liquid is added. Despite these structural reorganizations of the liquid, the plateau of mechanical stability extends by far the range where the liquid is solely present as individual capillary bridges. The mechanical stiffness of the wet pile decreases only for very large liquid content, corresponding to more than one half of the void space in the assembly being filled by liquid. This decrease of capillary cohesion

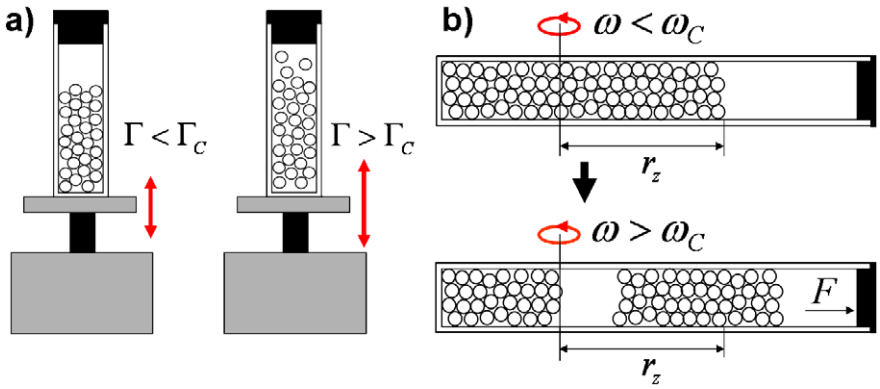

Figure 1. (a) Fluidization of a wet granulate by vertical agitation. The acceleration amplitude Γ of the harmonic oscillation is increased until the fluidization sets in at $\Gamma = \Gamma_c$. (b) Sketch of a centrifuge set up to measure the tensile strength of wet granulates. The angular velocity ω is increased until the granular column ruptures at $\omega = \omega_c$. The experiment has to be repeated for a number of distances r_z of the free end to the rotation axis.

may be responsible for sudden fluidizations of a wet granulate under external loads, in particular in response to shear stress. Such a fluidization behavior can be observed, for example, in certain types of landslides which occur after heavy rainfall. The present paper deals with the surprisingly wide extension of the above mentioned mechanical plateau region.

A systematic investigation of the complex behavior of wet granular assemblies has to cover several physical aspects ranging from the geometry of random packings [18–20] and capillarity [6, 8, 21] to the mechanics of cohesive granulates [2, 12, 14]. In general, the mechanical behavior of a wet granulate under tensile load, shear or compression will be linked to the local geometry of the grain in the assembly which governs the appearance of specific capillary states and transitions between them. In this article we will address the mostly unexplored interplay between capillary cohesion and wetting of complex geometries in partially saturated granulates [17]. The mechanical stiffness of mixtures between submillimetric glass beads and water are characterized by fluidization experiments and through tensile strength measurements. Furthermore, the morphology of the liquid clusters is investigated by x-ray microtomography and compared with numerically computed liquid shapes in ideal wetting geometries of monodisperse beads. A detailed discussion of some characteristic features of the packing geometry will lead us to a consistent picture, reconciling the structural data with the reported mechanical observations.

The article is organized as follows. In section 2 we introduce two experimental techniques which allow us to quantify the mechanical stability of wet assemblies of spherical glass beads. In addition, we explain the principles of fast x-ray microtomography as a technique to obtain three-dimensional images of the liquid clusters and the granular packing. Results of the mechanical tests and a classification of liquid shapes found in the microtomography images are presented and discussed in section 3. After a short summary in section 4 we conclude with a discussion of the impact of a wetting liquid on the mechanical behavior of a broader class of granulates, such as elliptical or irregular grains.

2. Experimental and methods

All mechanical tests and the x-ray microtomography were conducted with glass beads of different radii ranging from $R = 140$ μm to $R = 600$ μm with a relative polydispersity of $\delta R/R \approx 0.1$ purchased from Whitehouse Scientific Ltd, UK. Throughout our mechanical tests we used Millipore™ water as the wetting liquid. For the microtomography experiments, we added ZnI_2 to the water to obtain a higher contrast between the liquid phase and the glass beads. The liquid content of a wet granulate, W, is the defined as the volume of wetting liquid divided by the total volume the wet granulate. Similarly, the packing fraction of the granular assembly, ϕ, is the total volume of the beads divided by the sample volume. Hence the liquid content W in a random close packing of monodisperse beads with a packing fraction of $\phi_{\mathrm{rcp}} = 0.63$ [18] cannot exceed the value $W_{\mathrm{max}} = (1 - \phi_{\mathrm{rcp}}) = 0.37$.

2.1. Mechanical tests

In contrast to most composite solid materials such as alloys, fiber reinforced plastic or ceramics, it is rather difficult to measure the mechanical properties of a fragile material such as wet sand. Owing to the specific nature of wet granulates, we chose the fluidization threshold by vertical agitation and the tensile strength to characterize the cohesive strength of a wet granulate.

Vibrated wet granulates may behave like a fluid once the peak acceleration of the agitated container exceeds a certain value [22, 23]. This threshold value quantifies the collective effect of the cohesive forces between the grains. A sketch of a fluidization set up is shown in figure 1(a). Throughout our experiments we used cylindrical glass vials with a diameter of 2.8 cm which were mounted on a shaker. In all fluidization experiments the glass vials were vertically agitated at a frequency of 200 Hz. The peak acceleration was measured with an acceleration sensor. Samples were prepared according to two different protocols. According to the first protocol, the sample was compacted at a certain pressure before starting the fluidization measurement. In the

second protocol, the sample had been in a fully fluidized state before the agitation amplitude was slowly ramped down until solidification. The latter protocol leads to the formation of loose packings. In all measurements, the onset of fluidization was detected by visual inspection.

The maximum tensile load a granular packing can sustain provides a direct measure of the cohesive forces between the grains. Scheel *et al* showed that tensile stresses can be easily induced and measured with a centrifuge [17] (cf figure 1(b)). A small amount of the wet granulate was placed into a plastic tube (polyethylene) with a diameter of (3.0 ± 0.1) cm and mildly compacted with a piston at a pressure of (150 ± 50) kPa. The tube was then closed at one end and mounted horizontally on a rotation stage. When the tube is rotated around a vertical axis, the centrifugal potential gives rise to a tensile stress in the granulate which has a maximum close to the axis of rotation. At a certain threshold rotation frequency, the stress exceeds the tensile strength of the granulate, and the granular column ruptures. The tensile strength can be determined from the length of the free end of the granular column (r_z) and the rotation frequency at which rupture occurs. The experiment was repeated for a series of different r_z. In this way, the effects of the friction of the granulate with the wall of the plastic tube could be quantified and eliminated from the measurement of the tensile strength.

2.2. X-ray microtomography

X-ray microtomography was performed at beamline ID 15A of the European synchrotron radiation facility (ESRF) in Grenoble, France [24]. The microtomography set up consists of a rotation stage with a shaker (loudspeaker) mounted on it, a scintillator screen, and a fast CCD camera. Aqueous solutions of zinc iodide were used instead of pure water to increase the adsorption. Before a microtomogram was taken, the wet granulate was fully fluidized for a short time and given some time to equilibrate after solidification. This time was typically on the order of several hours. Around 800 absorption images (projections) were taken during a rotation of the sample by 180°. Owing to the high flux of the x-ray source, a full set of projections can be recorded in about 10 s. The spatial resolution of the two dimensional adsorption images is 14 μm. Finally, a three-dimensional gray scale image is computed from the series of projections using a reconstruction algorithm.

Subsequently, the three-dimensional gray scale images generated by the reconstruction algorithm were processed with the Mango toolkit [25]. This software package offers a variety of algorithms to segment the three-dimensional images into different phases [26] and to reduce noise levels [27]. Some regions of the images can be unambiguously assigned to certain phases by appropriate thresholding in the intensity–gradient space. The seed regions thus obtained employing a fast marching algorithm until they fill the entire image [28]. All further analyses of the segmented images were performed with custom made programs using Matlab™. In this way, we obtained the statistics of volume and surface area of individual liquid clusters, the angular distance of bead contact points, as well as the number of capillary bridges and liquid clusters in contact to a bead.

2.3. Numerical studies

Theoretical predictions for the liquid surface geometries can be obtained from a minimization of the interfacial energy. Throughout this work we made use of the program 'surface evolver' [29]. The liquid–air interface is modeled as a mesh of small triangles spanning between neighboring nodes. Local constraints are applied to the nodes of the three phase contact line since they have to glide on the surface of the beads. Locally stable configurations of the liquid–air interface are obtained by minimizing the total interfacial energy of the system using a standard conjugate gradient descent. Edge swapping and the removal or insertion of edges and nodes is applied to guarantee a constant quality of the mesh. The modeling of non-volatile liquid morphologies requires the condition of a constant liquid volume as a further, global constraint. The Lagrange multiplier of the latter is identical to the Laplace pressure, i.e. the pressure difference across the liquid–air interface. Furthermore, the capillary forces acting on individual spheres as well as the complete shape of a cluster can be obtained in a straightforward manner.

3. Results and discussion

Figures 2(a) and (b) display the results of our measurements of the fluidization threshold and the tensile strength of a homogeneous mixture of spherical glass beads with radius $R = (140 \pm 10\ \mu\text{m})$ and Millipore™ water. Both mechanical properties exhibit the same essential features: First, one observes a transition region up to a liquid content of approx. $W \simeq 10^{-3}$ where the mechanical stiffness increases dramatically. After this steep increase, the fluidization threshold and the tensile strength depend only weakly on the liquid content in the range from $W \simeq 5 \times 10^{-3}$ up to roughly $W \simeq 0.15$. A decrease of the mechanical stiffness is observed at fairly large liquid content, as far as measurements of fluidization and tensile strength are viable in this regime. Our measured values of the tensile strength of wet packings of glass beads are in good agreement with the values published by Pierrat *et al* [10], which span the range up to $W \approx 0.14$. In all fluidization experiments, i.e. for all bead radii and at all liquid contents under consideration, the agitation amplitude at the onset of fluidization is smaller than the diameter of the beads in the granulate.

Both mechanical tests presented here demonstrate that in the range of small liquid content, $W \leqslant 10^{-3}$, the capillary cohesion between spherical glass beads increases strongly with increasing W. This phenomenon is readily explained by the finite roughness of the bead surfaces. A certain amount of wetting liquid is bound to microscopic topographies, i.e. to dimples and troughs on the surface of the glass beads. As a consequence, a certain excess of liquid volume is required to form fully developed capillary bridges at the contact points between neighboring grains [2, 31]. The correlation between the onset of cohesion and capillary bridge formation has been previously confirmed by fluorescence microscopy [21, 22].

The constancy of the mechanical properties in the capillary bridge regime can be explained from the particular

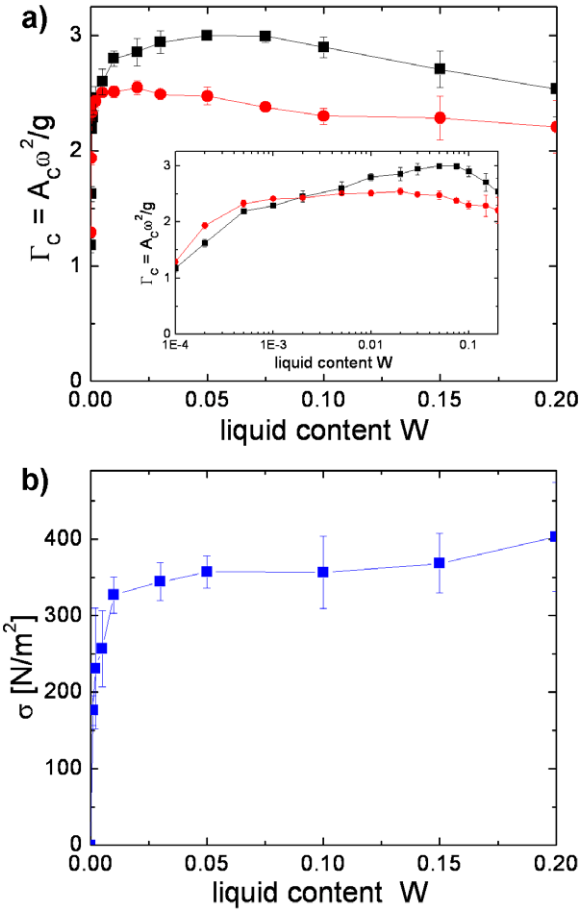

Figure 2. (a) Peak acceleration $\Gamma_c = A_c\omega^2$ at the onset of vertical fluidization, for spherical glass beads with radius 250 μm as a function of liquid content W. Squares refer to moderately compressed bead packings while the circles indicate the fluidizations threshold of previously fluidized samples. The amplitude and angular frequency of the oscillation is denoted, respectively, by Γ_c and ω. For liquid contents $W \gtrsim 2 \times 10^{-3}$, compressed bead packings show a larger fluidization threshold than re-fluidized samples. At larger contents the order is reversed. (b) Tensile strength σ of a wet granulate of glass beads at different liquid contents W measured with a centrifuge. The radius of the glass beads was $R = 140$ μm.

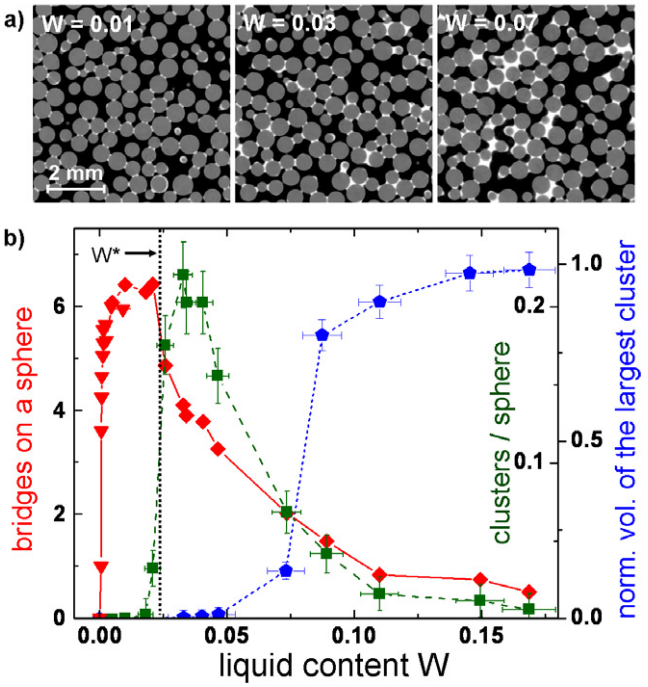

Figure 3. (a) Cross section of three-dimensional tomograms of wet glass beads at different liquid content W. Liquid and air appears as white, respectively, black areas while the glass beads appear as gray discs. (b) Cluster statistics as a function of liquid content W. Squares and triangles (red) refer to the average number of capillary bridges per bead. The circles denote the average number of clusters per bead. Pentagons indicate the volume fraction of the largest liquid cluster in the granulate.

scaling of the force with the liquid volume. It is well known that the force a capillary bridge induces between two spherical surfaces in contact tends to a finite value as the liquid volume of the bridge approaches zero [6–8]. The cohesive force of a large capillary bridges at zero separation, i.e. with a lateral extension being comparable to the bead radius, is almost identical to the asymptotic value at zero volume. The small variation of the capillary force over this extended range of volume has its origin in the particular scaling of the Laplace pressure and the wetted area in a spherical geometry [6–8]. This observation may well explain the plateau of the mechanical stiffness at small liquid contents $W < W^* \approx 2.4 \times 10^{-2}$ where individual capillary bridges predominate.

Figure 3 shows the number of capillary bridges and liquid clusters, i.e. distinct domains of the liquid being in contact with three or more beads, and the volume of the largest cluster as functions of the liquid content[5]. It is apparent that the morphology of the liquid domains undergoes large changes in the displayed range of liquid content. As W is increased, individual capillary bridge coalesce and form larger clusters. At a liquid content of $W = 0.11$ we find that the largest cluster comprises about 90% of the entire liquid volume in the sample (cf figure 3). The results furthermore suggest a percolation transition around $W \approx 0.08$.

As already observed for the mechanical stiffness of the granulate, the number of bridges per bead displays a plateau at a value $N_b \simeq 6.4$ above a liquid content $W > 5 \times 10^{-3}$. In ideal random packings of perfectly round and impenetrable beads one expects that the number of capillary bridges equals the value of the number of contacts, in the frictionless isostatic case $N_b = 6$ [30]. The discrepancy between the number of bridges and mechanical contacts per bead can be explained by two effects. On the one hand beads which are not perfectly spherical must have a higher number of contacts in a stable mechanical equilibrium [19]. On the other hand, capillary bridges may be found at a pair of adjacent beads with a finite separation, i.e. neighbors which are not in mechanical contact. In contrast to the tensile strength and fluidization threshold this plateau in the number of bridges per sphere is limited by a sharp decay at a characteristic liquid content $W^* \approx 2.4 \times 10^{-2}$. At the same point, the number of liquid clusters in

[5] A capillary bridge is defined as a liquid domain being in contact with exactly two neighboring beads.

the sample, i.e. liquid domains in contact with more than two beads, increases. This clearly indicates that W^* relates to the onset of coalescence of capillary bridges.

The liquid clusters formed in this coalescence process can be characterized by their total interfacial area, S, and volume, V. Each single point in the plot shown in figure 4 represents a single liquid cluster in a microtomography image taken at a liquid content of $W = 3.5 \times 10^{-2}$. A dense group of data points at small surface areas and small liquid volumes can be assigned to isolated capillary bridges. At larger values of S and V, several distinct point clouds corresponding to larger liquid clusters are visible. Close inspection of the x-ray microtomography images reveals that the clusters belonging to a certain cloud of data points can be identified with a particular class of morphologies. The insets of figure 4 display the generic cluster morphologies assigned to the corresponding clouds of data points. Quite surprisingly, the morphology of most liquid clusters falls into a small number of classes. For the capillary bridges, trimers, pentamers, and tetrahedra, the numerically obtained cluster geometry is shown for comparison.

Moreover, the surface over volume plot in figure 4 reveals that the data points follow an almost linear scaling relation at larger volumes. Such linear scaling between the surface and volume is expected for compact liquid structures, i.e. spatial regions of the packing whose void space is entirely filled with liquid. The corresponding prefactor of the linear relationship can be directly computed from the radius of the glass spheres, R, and the packing fraction, ϕ. With the total surface area of the beads, $S = 4\pi N R^2$, their number $N = 3V_0\phi/4\pi R^3$, and the volume of the void space between the beads $V = (1-\phi)V_0$, one finds a surface-to-volume ratio $S/V = 3\phi/R(1-\phi)$. The corresponding linear scaling is indicated by the solid line in figure 4. This value represents the smallest surface-to-volume ratio of a liquid domain that can be attained in a granular assembly of monodisperse spheres at a given packing fraction ϕ and bead radius R. The dashed line in figure 4 displays the surface-to-volume ratio of a percolating liquid cluster for a sample with the same bead radius but at an elevated liquid content of $W = 0.11$ with a surface area $S = 8.2 \times 10^6$ pixel and volume $V = 5.3 \times 10^6$ voxel. The surface-to-volume ratio of the percolating cluster is more than 3.6 times larger than what would be expected from a region in the granular assembly being fully saturated by liquid.

3.1. Cluster formation

To explain the large surface-to-volume ratio of large liquid clusters we have to take a closer look at the process of their formation. If we consider an ideal triangular configuration of three spherical beads in mutual contact and assume that two neighboring capillary bridges have the same Laplace pressure, their opening angle β will be limited to values below 30°. Larger opening angles can be excluded since the capillary bridges, while growing, would touch and eventually coalesce. Employing simple geometrical arguments the corresponding Laplace pressure p of a capillary bridge can be obtained from a toroidal approximation of the liquid–vapor interface,

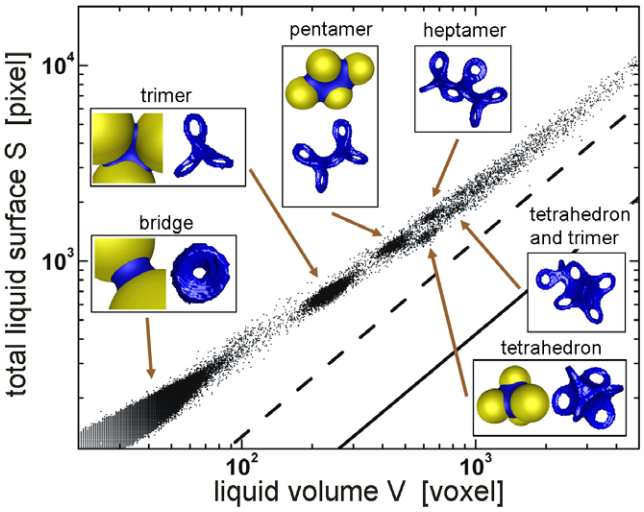

Figure 4. Data collapse of surface area S and liquid volume V of liquid clusters found in a three-dimensional x-ray microtomography image. The dashed line corresponds to the surface area to volume ratio of the largest liquid cluster in the sample. The solid line indicates the ratio of bead surface area to the volume of the packing. Insets: comparison between numerically obtained liquid shapes and generic cluster morphologies found by x-ray microtomography.

see [6, 8, 17]. Assuming perfect wetting, i.e. the contact angle of the liquid with the surface of the beads is zero, the Laplace pressure of a 'critical' capillary bridge with an opening angle $\beta^* = 30°$ equals $p^* = -(1+2\sqrt{3})\gamma/R \approx -4.46\gamma/R$ [17].

Once three capillary bridges located at such a triangular configuration touch each other and coalesce, the triangular opening between the beads will be filled by liquid. Owing to the trifold geometry, the final liquid morphology, i.e. after coalescence is completed, has been termed a *trimer* (cf see figure 4). Except for the central part, the shape of a trimer is almost identical to the three capillary bridges provided the Laplace pressure of the bridges and the trimer are identical. The Laplace pressure of a trimer at the same volume, however, is smaller than the Laplace pressure of the three bridges prior to coalescence.

A statistical analysis of the microtomography data demonstrates that local triangular configurations of three neighboring beads appear in abundant levels in dense random packings of spherical beads. The distribution of angular distances between bead contacts is shown in the inset of figure 6. The distribution exhibits a sharp peak at $\alpha = 30°$ while angular distances smaller than 30° are virtually absent. A second, broad maximum can be observed at an angular distance of close to 60°.[6] The liquid content W^* which separates the regime of individual capillary bridges from the regime of liquid clusters can be computed from the volume of a capillary bridge with an opening angle $\beta^* = 30°$, the number of contacts per spheres being $N_c = 6.4$, and the packing fraction $\phi = 0.58$ of the wet granulate. The calculated value of $W^* = 2.4 \times 10^{-2}$

[6] Due to the finite resolution of the x-ray microtomography images we had to introduce a threshold separation δs to decide whether two neighboring beads are in contact or not. The shape of the distribution, however, is hardly affected by the value of δs.

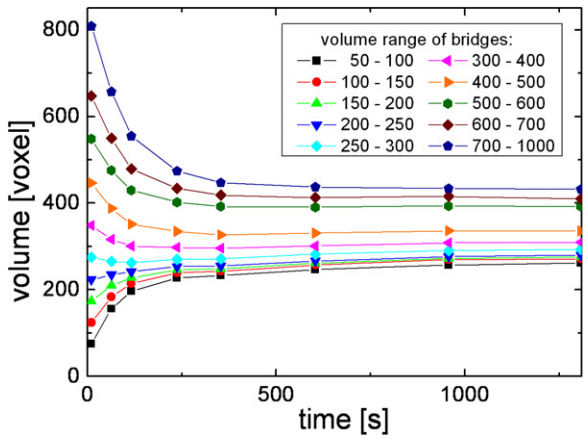

Figure 5. Volume of individual capillary bridges as a function of the time elapsed after stopping agitation. Each of the bridge volumes exhibits an exponential relaxation toward an asymptotic value with a time constant of several minutes.

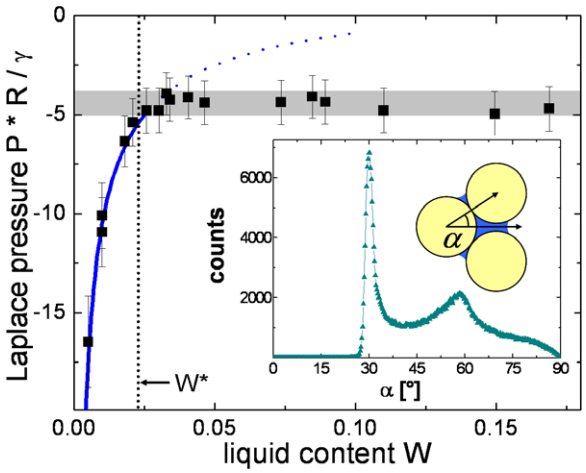

Figure 6. Laplace pressure p, normalized by the ratio of interfacial tension γ and bead radius R, of individual capillary bridges in an assembly of glass beads as a function of liquid content W. The Laplace pressure was computed from the volume of isolated capillary bridges at zero separation and assuming perfect wetting. The gray bar corresponds to the range of critical Laplace pressures p^* for contact angles between 0° and 15°. Inset: distribution of angular distances between pairs of contact points on a bead.

is in perfect agreement with the experimentally obtained value for the onset of cluster formation (cf also figure 3).

Because a spherical bead in the random assembly is part of not only one but of several local triangular configurations, trimers or capillary bridges may merge with other capillary bridges or trimers, leading to pentamers, heptamers, and larger aggregates of capillary bridges. Examples of smaller capillary bridge 'polymers' are shown in the inset of figure 4. Besides the trimer as a fundamental motif, we observed clusters that correspond to six capillary bridges which have coalesced in the tetrahedral gap formed by four spherical beads. The fused capillary bridges which form a cluster appear as loops in the x-ray microtomograms. This artifact can be explained by the finite resolution of the images. Close to the point of bead contact the thickness of the liquid film falls below the resolution limit and the bridges and clusters appear perforated. Because the shape of such a loop is close to the shape of an isolated bridge, the limiting Laplace pressure at coalescence between a liquid cluster and other liquid clusters or bridges is expected to be equal to p^*.

This prediction is confirmed by indirect measurements of the Laplace pressure as follows. The high intensity of the x-ray beam at the ESRF allowed us to track the volume of certain liquid structures in the packing over a period of several minutes with a time resolution of ∼10 s. Figure 5 displays the volume of a number of individual liquid bridges as a function of time which had elapsed since the agitation of the sample was stopped. A relaxation of the individual bridge volumes to an asymptotic value can be observed with a characteristic time of approximately 5 min. This can be explained by an exchange of aqueous ZnI_2 solution between different liquid volumes. This observation strongly indicated that the Laplace pressure is the same in all capillary bridges and liquid clusters. From the size of the capillary bridges, some of which are found in almost all samples, we can thus infer the Laplace pressure in all of the liquid clusters in the sample. Here, we used the toroidal approximation to analytically calculate the Laplace pressure of a capillary bridge as a function of its volume. As shown in figure 6, we indeed find the predicted pressure p^* in the liquid clusters for all values of the liquid content above W^*.

Consecutive fusion of capillary bridges and the corresponding filling of the triangular openings leads to rather open liquid morphologies, just as observed in the experiments. The extension of the plateau in the mechanical stiffness from the regime of individual capillary bridges into the cluster regime can be understood from the coalescence process and the resulting morphologies. On the one hand, the area over which the Laplace pressure acts on the spherical beads and the length of the three phase contact line remain almost unchanged during an increase of W. On the other hand, the Laplace pressure p is effectively fixed by the local geometry in the granulate to a value p^*. As a consequence of the Laplace pressure p being limited to p^* in the coalescence regime, pores in the assembly with a radius larger than the radius of the triangular opening cannot be filled by liquid unless p exceeds p^*. A further increase of the Laplace pressure towards less negative values should be observable once all triangular openings are filled by liquid. The liquid content at this point may coincide with the range of W where the cohesive stress in the granulate again weakens.

4. Conclusions and outlook

The insensitivity of mechanical stability of a wet granulate with respect to the liquid content was demonstrated for mixtures of spherical beads and water in measurements of the fluidization threshold by vertical agitation and of the tensile strength. In addition to the cohesive strength of a wet granulate, we have studied the equilibrium shapes of wetting liquids in static granular assemblies of spherical glass beads. High resolution x-ray microtomography and the application of efficient segmentation algorithms allowed us to resolve the packing geometry of the grains and the shape of the

liquid structures in three dimensions with a sufficient spatial resolution. Equilibration of the liquid in the granulate could be monitored because of the high temporal resolution of the microtomography set up.

As expected, we found a regime of liquid contents $W < W^* = 2.4 \times 10^{-2}$ where the capillary bridges are exclusively found. Characteristic liquid clusters appear at liquid contents above W^*, the most fundamental being a trimer of three capillary bridges joined together at a triangular opening formed by three adjacent spherical beads. Consecutive fusion of capillary bridges in triangular sites lead to the formation of larger ramified aggregates which consist mainly of trimer building blocks. Arrangements of six capillary bridges arranged around a tetrahedral gap have been found in smaller numbers. All experimentally detected liquid shapes could be directly compared to the results of numerical minimizations of the interfacial energy in the respective bead geometries.

Let us finally discuss what we should expect when using non-spherical grains instead of the glass spheres used so far. What will definitely change is the average number of contacts between adjacent spheres, and hence the number of capillary bridges. For completely aspherical grains one may expect twelve contacts instead of six. We thus expect, qualitatively, that deviations from the spherical shape give rise to a stronger cohesion due to the increased number of capillary bridges. A quantitative estimate also requires a consideration of the individual capillary bridges, since their geometry will no longer be identical to what we have found for spherical beads. However, if we assume the grains to be sufficiently smooth, we can gain additional results. The proximity of a contact between two convex, twice differentiable bodies is always equivalent to a contact between two spheres, as far as the separation of the two surfaces as a function of the distance from the contact point is concerned [7]. For a discussion of interparticle forces, we can thus consider the bridges at these contacts as spanning between two spheres the radii of which are equal to the average mean curvature of the touching bodies at their point of contact. If we assume that the mean curvatures at the contact points average out in the ensemble to the mean curvature averaged over a single grain, we come to the conclusion that the capillary bridges between the non-spherical grains should exert similar forces, on average, as those between spheres of the same volume as the grains. Owing to the larger number of bridges per grain, we furthermore expect that the critical angle at which neighboring bridges coalesce will be smaller than for spheres, but it will again, averaged over the pile, be well defined. The Laplace pressure will thus be larger in the clusters which form, but the cohesive force per capillary bridge will be similar. As a conclusion, we expect that the stiffness of the wet granular pile will roughly scale with the number of contacts between grains, which is solely determined by their shape. The wide plateau in the mechanical stiffness is expected to be present as well. In fact, we have repeated our mechanical test with regular sand instead of glass beads, and we find the same wide plateau in the critical fluidization, but at a somewhat higher level [32]. This collaborates our reasoning above.

References

[1] Hornbaker D J, Albert R, Albert I, Barabasi A-L and Schiffer P 1997 *Nature* **387** 765
[2] Halsey T C and Levine A J 1998 *Phys. Rev. Lett.* **80** 3141–4
[3] Nowak S, Samadani A and Kudrolli A 2005 *Nat. Phys.* **1** 50–2
[4] Schiffer P 2005 *Nat. Phys.* **1** 21–2
[5] Lu N, Wu B and Tan C P 2007 *J. Geotech. Geoenviron. Eng.* **133** 144–54
[6] Fisher R A 1926 *J. Agric. Sci.* **16** 492–505
[7] Israelachvili J N 1992 *Intermolecular and Surface Forces* (London: Academic)
[8] Willett C D, Adams M J, Johnson S A and Seville J P K 2000 *Langmuir* **16** 9396–405
[9] Rumpf H 1962 *Agglomeration* (New York: AIME, Interscience)
[10] Pierrat P and Caram H S 1997 *Powder Technol.* **91** 83–93
[11] Bocquet L, Charlaix E and Restagno F 2002 *C. R. Physique* **3** 207–15
[12] Gröger T, Tüzün U and Heyes D M 2003 *Powder Technol.* **133** 203–15
[13] Richefeu V, El Youssoufi M S and Radjaï F S 2006 *Phys. Rev.* E **73** 051304
[14] Soulié F, El Youssoufi M S, Cherblanc F and Saix C 2006 *Eur. Phys. J.* E **21** 349–57
[15] Herminghaus S 2005 *Adv. Phys.* **54** 221–61
[16] Mitarai N and Nori F 2006 *Adv. Phys.* **55** 1–45
[17] Scheel M *et al* 2008 *Nat. Mater.* **7** 189–93
[18] Bernal J D 1960 *Nature* **185** 68–70
[19] Donev A *et al* 2004 *Science* **303** 990–3
[20] Aste T 2006 *Phys. Rev. Lett.* **96** 018002
[21] Kohonen M M, Geromichalos D, Scheel M, Schier C and Herminghaus S 2004 *Physica* A **339** 7–15
[22] Scheel M, Geromichalos D and Herminghaus S 2004 *J. Phys.: Condens. Matter* **16** S4213–8
[23] Fournier Z *et al* 2005 *J. Phys.: Condens. Matter* **17** S477–502
[24] Di Michiel M *et al* 2005 *Rev. Sci. Instrum.* **76** 043702
[25] Averdunk H and Sheppard A 2007 http://xct.anu.edu.au/mango
[26] Sheppard A P, Sok R M and Averdunk H 2004 *Physica* A **339** 145–51
[27] Frangakis A S and Hegerl R 2001 *J. Struct. Biol.* **135** 239–50
[28] Sethian J A 1999 *Level Set Methods and Fast Marching Methods: Evolving Interfaces in Computational Geometry, Fluid Mechanics, Computer Vision and Materials Science* (Cambridge: Cambridge University Press)
[29] Brakke K 1996 *Phil. Trans. R. Soc.* A **354** 2143–57
[30] Moukarzel C F 1998 *Phys. Rev. Lett.* **81** 1634–7
[31] Tegzes P, Vicsek T and Schiffer P 2002 *Phys. Rev. Lett.* **89** 094301
[32] Scheel M *et al* 2008 in preparation